Beam Plasma Expansion of a Helicon Plasma Source

IEPC-2019-434
Presented at the 36thInternational Electric Propulsion Conference
University of Vienna • Vienna, Austria
September15-20, 2019

Zun Zhang[1] and Haibin Tang[2]
Beihang University, Beijing, 100083, China

and

Kan Xie[3] and Jiting Ouyang[4]
Beijing Institute of Technology, Beijing,100081, China

Abstract: An optical emission spectrometer with a spatial resolution of 5 mm has been used for the determination of the spatial distribution of the beam plasma parameters and its variation with different input RF powers (100-1000 W) and diameters of the discharge tube (20-60 mm). Measured results show that the electron density decrease with both axial and radial distances but the electron temperature remains nearly constant with both axial and radial distances, which indicating that the beam plasma of the helicon source follows the isothermal (Boltzmann) expansion. Furthermore, the electron density increases with increasing input RF powers because of an increase of power deposition. The radial profiles of electron density become flat and the centerline maximum electron densities decrease with increasing diameters of the discharge tube because of a decrease of the power density.

Nomenclature

A	=	effective collecting area of the probe
A_{ji}	=	optical emission probability
c	=	speed of light
E_i	=	threshold energy of the lower lines
E_j	=	threshold energy of the upper lines
e	=	electron charge
$f(v,T_e)$	=	electron distribution function
g_{ji}	=	statistical weight of the emission
h	=	Planck constant
I_{Bohm}	=	Bohm current
I_{total}	=	probe current
I_{ji}	=	emission intensity
I_{sat}	=	ion saturation current
K_{ji}	=	a factor depending on the plasma volume
k	=	Boltzmann constant
$k_{\mathrm{Ar}}^{\mathrm{dir}}$	=	direct electronic excitation rate coefficient
$k_{\mathrm{Ar}}^{\mathrm{rad}}$	=	spontaneous radiation rate coefficient
m_e	=	electron mass
m_i	=	ion mass

[1] Lecturer, School of Space and Environment, Beihang University, and zhangzun@buaa.edu.cn.
[2] Professor, School of Space and Environment, Beihang University, and thb@buaa.edu.cn.
[3] Professor, School of Aerospace Engineering, Beijing Institute of Technology, and xiekan@bit.edu.cn.
[4] Professor, School of Physics, Beijing Institute of Technology, and jtouyang@bit.edu.cn.

n_{Ar}	=	density of ground state particles
n_{Ar*}	=	density of excited state particles
n_e	=	electron density
T_e	=	electron temperature
V_p	=	probe voltage
v	=	electron velocity
τ	=	lifetime of the excited state
λ_{ji}	=	wavelength of the transition
$\sigma(v)$	=	effective excitation cross section

I. Introduction

THERE is growing interest in utilizing helicon plasmas in space propulsion as a thruster or a component thereof due to their advantages of electrodeless, high density, multiple operation mode and so on. There are two approaches to helicon thrusters: a single-stage device that creates and accelerates ions simultaneously (for example the Helicon Double Layer Thruster, HDLT) [1-5], or a two-stage device that separates ionization and ion acceleration (for example the Variable Specific Impulse Magnetoplasma Rocket, VASIMR®) [6-8].

For both single- and two-stage helicon thrusters, the spatially resolved beam plasma properties of the single-stage thruster are very important because it is the beam plasma that directly form the thrust of the single-stage thruster and its properties are the input parameters of the two-stage helicon thruster.

Many efforts have been made by Christine Charles and Rod Boswell, Logan Todd Williams, Takahashi and so on. Charles and Boswell used a retarding field energy analyzer (RFEA) and a Langmuir probe to figure out the spatial evolution of the plasma potential, electron temperature, electron density and ion energy. They concluded that the measured electron temperature was approximately constant along the z-axis at about 3.9 eV for Argon therefore the plasma downstream has been shown to follow a Boltzmann expansion [9]. Williams used an emissive probe and a Langmuir probe to map the 2-D contour of the plasma potential, electron density and electron temperature. He concluded that the electron number density rapidly decreases downstream of the exit plane by more than an order of magnitude and the electron temperature first increases and then decreases monotonically as the axial position increases [10]. Takahashi used a Langmuir probe to get the radial profiles of the electron density with different pulsed applied magnetic field. He concluded that plasma radius can be slightly decreased by the stronger magnetic field because the radial diffusion across the magnetic field can be suppressed by the strong magnetic field and the plasma is more efficiently focused there [11].

Usually, the spatially resolved electrostatic probes such as Langmuir probe have been used to measure the beam plasma characteristics. But it works difficult when the RF input power and the applied magnetic field is very high. For example, the Langmuir probe shows distorted I-V curves and falsely high value of T_e when the RF input power is higher than 1 kW and when the discharge is on a transition stage between two modes. The optical emission spectroscopy (OES) is affected little by the high frequency electrostatic field and high applied magnetic field. However, it has not been used for a radially resolved measurement of the plasma parameters because it usually collects all the photo numbers integrated along the line of sight.

In order to make the optical emission spectroscopy (OES) have a good spatial resolution, we newly designed a ceramic mechanism on the head of the optical sensor. This new design makes the optical spectrometer have a spatial resolution of 5 mm and could be immersed in the plasma by an optical cable crossing the vacuum chamber. This will help us getting the 2-D map of the electron temperature and electron density and furthermore their variations with different input RF powers and diameters of the discharge tube. Although the OES assembly is kind of invasive it still has many advantages. Firstly, it can separate the integrated line of sight into small sections like 5 mm or even smaller to achieve a radial resolution. Secondly, it collects the photo numbers not the charged particles in plasma therefore the plasma potential oscillations resulted from the RF source has no influence on it. Thirdly, it has no high voltage scan like Langmuir probe so it has no interference to the electrodes therefore it especially suits for plasmas diagnostics in very small region or near wall region.

The paper is organized in the following way: the optical emission spectroscopy diagnostics is described in Sec. II; the experimental apparatus including the vacuum chamber, helicon source, solenoidal coil and OES diagnostic arrangement are presented in Sec. III; the plume plasma test results are shown in Sec. IV; the conclusions are summarized in Sec. V.

II. Diagnostics

A. Optical Emission Spectroscopy

The Corona model has been used to establish a relationship between the optical emission intensity and the electron density. The electron temperature has been calculated from the line-ratio method. The corona model has been successfully tested in electrodeless RF discharges in pure Ar and N_2 in the pressure range from 0.1 to 1 Pa, with the electron temperature vary between 2-10 eV and electron density of 10^{15} m^{-3} up to 10^{17} m^{-3} [12-13].

In the Corona model the excitation to any emitting state is assumed to result from the collision between a plasma electron of sufficient energy and a neutral ground state particle.

① **Direct excitation** by electron collision from the ground state of Ar:

$$e + Ar \rightarrow e + Ar* \qquad (k_{Ar}^{dir}) \tag{1}$$

where k_{Ar}^{dir} is the rate coefficient for direct electronic excitation from the ground state.

The spontaneous decay of excited states is regarded as the only response in the Corona model to balance the electron impact excitation processes. Other effects such as from heavy particle interactions are assumed to become negligible in the present case because of the low particle densities. Also, radiative ion-electron recombination can be neglected at a low ionization degrees as 10^{-3} to 10^{-2} [12].

② **Radiative de-excitation**:

$$Ar* \rightarrow Ar + h\nu \qquad (k_{Ar}^{rad}) \tag{2}$$

where k_{Ar}^{rad} is the rate coefficient for spontaneous radiation of the excited state, and

$$k_{Ar}^{rad} = 1/\tau \tag{3}$$

τ is the lifetime of the excited state.

Under such simplifying assumptions described above, the balance between the production of an excited state and its decay can be expressed by

$$n_e n_{Ar} k_{Ar}^{dir} = n_{Ar*} k_{Ar}^{rad} = \frac{n_{Ar*}}{\tau} \tag{4}$$

where n_e is the electron density (cm^{-3}), n_{Ar} is the density of ground state particles (cm^{-3}), n_{Ar*} is the density of excited state particles (cm^{-3}), k_{Ar}^{dir} is the rate coefficient for direct electronic excitation from the ground state (cm^3 s^{-1}), and τ is the lifetime of the excited state (s^{-1}).

For an excited Ar^*, the emission intensity I_{ji} due to a transition from an upper level j to a lower state i is

$$I_{ji} = K_{ji} A_{ji} n_{Ar*} \frac{hc}{\lambda_{ji}}, \tag{5}$$

where K_{ji} is a factor depending on the plasma volume, solid angle and spectral response of the spectrometer, A_{ji} is the optical emission probability for the transition (s^{-1}), n_{Ar*} is the density of the excited species (cm^{-3}), c is the speed of light (ms^{-1}), h is the Planck constant (J·s) and λ_{ji} is the wavelength of the transition (nm).

By using equation (4), it follows that:

$$I_{ji} = K_{ji} A_{ji} \frac{hc}{\lambda_{ji}} n_e n_{Ar} k_{Ar}^{dir} \tau \tag{6}$$

In low density plasmas, the electron temperature (determine k_{Ar}^{dir}) and ground state particle density n_{Ar} can often assumed to be constant in the plasma volume [12]. Therefore, except the electron density n_e, the coefficients on the right side of equation (6) can be determined to be a constant value at a definite emission line. In that way, equation (6) can be simplified as

$$I_{ji} = K n_e \text{ or } n_e = k I_{ji} \tag{7}$$

Thus, we establish a linear relationship between the emission intensity and the electron density. This means that the emission intensity could represent the "relative" electron density, or the "absolute" density if the coefficient "k" can be calibrated by the electron density derived from a RF compensated Langmuir probe.

This relationship has also been mentioned by K. Behringer in his paper that: "all line intensities are proportional to the electron density." [12]

The electron temperature T_e enters equation (6) via the rate coefficient k_{Ar}^{dir}

$$k_{Ar}^{dir} = \int_0^\infty f(v, T_e) v \sigma(v) dv \tag{8}$$

with $f(v,T_e)$ being the electron distribution function, v being the electron velocity and $\sigma(v)$ being the corresponding effective excitation cross section.

A Maxwellian electron energy distribution was assumed [14]

$$f(v,T_e)=\left(\frac{m_e}{2\pi kT_e}\right)^{\frac{3}{2}}\exp\left(-\frac{m_e v^2}{2kT_e}\right) \tag{9}$$

where m_e is the electron mass and T_e is the Maxwellian electron temperature.

The effective excitation cross section $\sigma(v)$ can be calculated by [15]

$$\sigma(v)=\frac{\pi e^4 g_{ji}}{\left(\frac{1}{2}mv^2\right)\left(E_j-E_i\right)} \tag{10}$$

where e is the electron charge, m is the electron mass, v is the electron velocity, g_{ji} is the statistical weight of the emission, E_i and E_j are the threshold energy of the lines.

As for the determination of the electron temperature T_e, the emission line ratio method was used. The intensity of an individual emission line can be calculated from equation (6). If we choose a pair of individual emission lines, their intensity ratio can be calculated from equation (11) as a function of the electron temperature T_e.

$$\frac{I_{qp}}{I_{ji}}=\left(\frac{\lambda_{ji}A_{qp}g_q}{\lambda_{qp}A_{ji}g_j}\right)\exp\left(\frac{E_j-E_q}{kT_e}\right) \tag{11}$$

Here, I_{qp} and I_{ji} are the emission intensity of two different emission lines, λ_{qp} and λ_{ji} are the wavelength of the emission lines, A_{qp} and A_{ji} are the optical emission probability for the emission lines, g_q and g_j are the statistical weight of the upper level of the emission lines, E_q and E_j are the threshold energy of the two emission lines, k is the Boltzmann constant, and T_e is the electron temperature.

Also, equation (11) could be written as

$$kT_e=\left|\left(E_j-E_q\right)\left[\ln\left(\frac{I_{qp}\lambda_{qp}A_{ji}g_j}{I_{ji}\lambda_{ji}A_{qp}g_q}\right)\right]^{-1}\right| \tag{12}$$

Thus, if we obtained the intensity ratio of two emission lines from an experiment and found the corresponding coefficients of E_j, E_q, λ_{qp}, λ_{ji}, A_{qp}, A_{ji} g_q, and g_j, from the reference of [16], the electron temperature T_e could be determined by equation (12) [17-18].

The accuracy of the T_e and n_e results derived from the OES method is limited by the uncertainties in the relevant rate coefficients, simplified reaction process and, to some extent, by the reproducibility of the plasmas. At low pressures, this is another non-negligible source of error. Realistic error bar for T_e from the line ratio method is probably about 20%, while just an indication of the magnitude for n_e [12].

B. RF compensated Langmuir Probe

The absolute electron density is calibrated by a commercial RF compensated single Langmuir probe which is made by the Impedans Ltd. The detailed data processing method for a Langmuir probe can be found in references [19] and [20]. The electron temperature and density are derived from equations (13) and (14), respectively.

$$T_{ev}=\frac{V_p}{\ln(I_{total}-I_i)}\approx\frac{V_p}{\ln(I_e)} \tag{13}$$

$$n_e=\frac{I_{Bohm}}{eA0.61}\sqrt{\frac{m_i}{kT_e}}=\frac{I_{sat}}{eA0.61}\sqrt{\frac{m_i}{kT_e}} \tag{14}$$

where T_{ev} is the electron temperature (eV), V_p is the probe voltage (V), I_{total} is the probe current (A), I_{sat} is the ion saturation current (A), I_{Bohm} is the Bohm current (A), n_e is the electron density (m^{-3}), e is the electron charge (1.6×10^{-19} C), A is the effective collecting area of the probe (m^2), k is the Boltzmann constant (1.38×10^{-23} J/K), T_e is the electron temperature (K), and m_i is the ion mass (kg).

Considering a typical electron density in our research is 5×10^{17} m^{-3} and electron temperature is 3 eV, the Debye length calculated is 0.018 mm compared with the probe radius of 0.15 mm. The ratio of the probe radius to the

Debye length is nearly 10. Therefore, the classical data reduction process of the thin sheath theory for the single Langmuir probe was used; the experimental errors for the electron temperature and density are estimated of 20% and 50%, respectively [21-23].

III. Experimental Apparatus

The experimental set-up is shown in figure 1. It consists of a 20 mm diameter 450 mm long quartz tube for the plasma discharge, which surrounded by two axial solenoids and attached to a 500 mm long 300 mm diameter earthed stainless steel diffusion chamber. The closed end of the tube is sealed by a dielectric plate (polytetrafluoroethylene, PTFE). The quartz tube could be changed to 40 or 60 mm diameter tube with a corresponding diameter antenna. A 155 mm long water-cooled helical antenna surrounds the quartz tube. The antenna connects to a 13.56 MHz RF source. A divergent magnetic field decrease from about 0.02 T (200 G) in the source center to about 0.001 T (10 G) in the middle of the diffusion chamber. The magnetic field is generated using equal currents of 40 A in the two axial solenoids. The mass flow rate of argon propellant is 8.8 sccm (standard cubic centimeter per minute) during the discharge. The system is pumped down to a base pressure of 10^{-3} Pa using a turbo-molecular-rotary pumping system connected to the side of the diffusion chamber. The working pressure was about 0.4 Pa (3 mTorr) and was measured with an ionization gauge. The crossover density calculated is 1.9×10^{11} cm^{-3} by the equation of $n_{crit}\approx6.9\times10^{19}\, P_{mTorr}T_{eV}^{2}$ cm^{-3} for P_{mTorr} = 3 mTorr and T_{eV} = 3 eV where P_{mTorr} is the working pressure and T_{eV} is the electron temperature. The crossover density still belongs to the low density range and therefore the plasma is still controlled by electron-neutral collisions. An OES made by Avantes Company was used for the spatial diagnostics. The wavelength range of the OES is 200-900 nm. The spatial resolution of the OES is 5 mm due to a special design, which has been described in detail in our previous work [18]. For a brief description here, as shown in figure 2, a ceramic tube has been designed so that only a small part of the plasma (5 mm long) could enter the hole at the head of the tube. The crossing area, the red area as shown in figure 2, of the entered plasma and the integrated line of sight is the spatially resolved plasma area for the OES assembly. With a moving holder for this OES assembly, the spatial electron temperature and density could be determined. In our work the OES assembly is fixed to a 2D moving mechanism to get to the planned measurement locations.

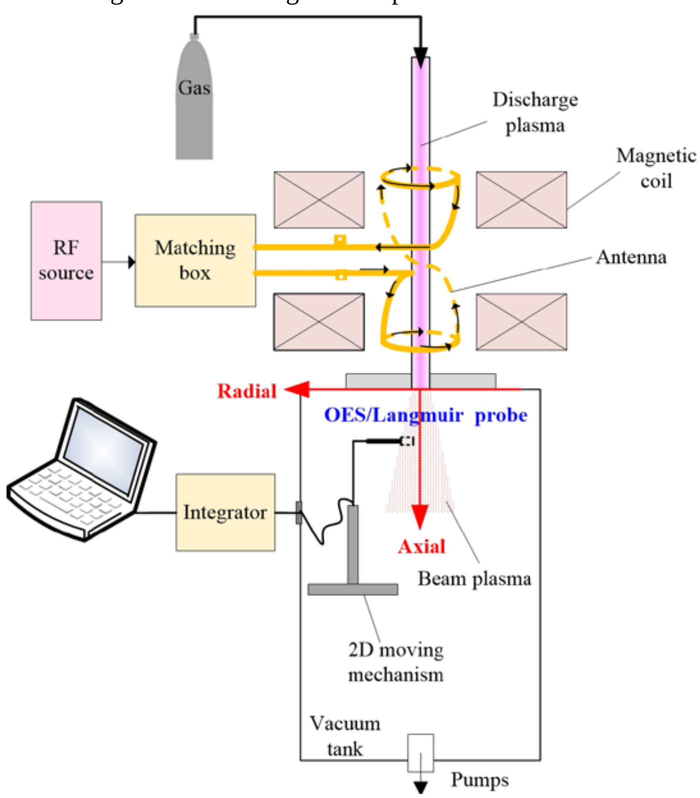

Figure 1. Global sketch of the Helicon plasma source, vacuum chamber and diagnostics

The single RF compensated Langmuir probe immersed in the beam plasma is mounted on the 2D moving mechanism to measure the spatial plasma characteristics. The diameter of the tungsten probe is 0.3 mm and its length is 8 mm. The bias voltage is from -100 to +100 V at a frequency of 1 Hz.

Probe positioning was maintained by the 2D moving mechanism which is powered by two step-motors. The mechanism consists of two movement stands inside the vacuum tank, and two servo control windows outside the vacuum tank. Each movement stand can move the probe within a 110 mm range.

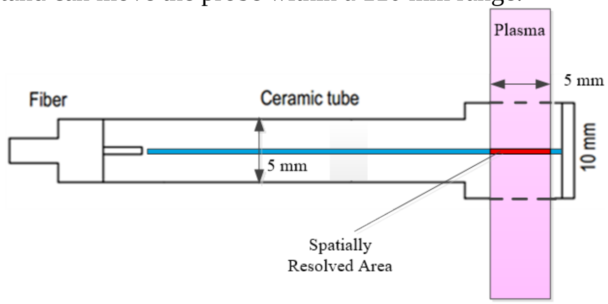

Figure 2. Design detail of the spatially resolved OES.

IV. Experimental Results

A. Electron Density Calibration

Because the performance of the Langmuir probe degrades a lot (giving distorted I-V curves and falsely high value of T_e) when the RF input power is higher than 1 kW and when the discharge is on a transition stage between two modes, we tried to build a relationship between electron density and the intensity of the OES emission lines since the optical method is independent of electric and magnetic field during the RF discharge.

According to the Corona model described above, as shown in equation (6), all emission line intensities are proportional to the electron density. That is means all emission line intensities can represent the relative electron density.

Figure 3 shows the emission spectra of an argon discharge, which shows that the wavelengths of the emission lines with the highest intensity are 811.5311 nm line and 750.3869 nm line. Therefore, we choose the intensity of 811.5311 nm line and 750.3869 nm line to represent the relative electron density and use their ratio to calculate the electron temperature for a higher ratio of signal to noise. Furthermore, we use the electron density derived from the RF compensated single Langmuir probe to calibrate the relative electron density derived from the OES emission intensities. Most of the important, we have to conform whether the electron density and the emission intensity have the linear relationship as predicted in the Corona model and if so determine the value of k in equation (7).

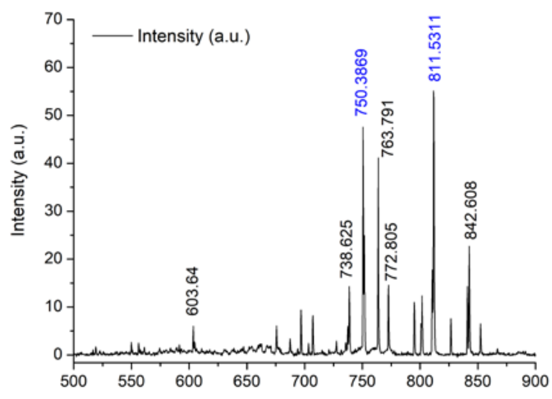

Figure 3. Emission spectra of an argon discharge.

Figure 4 shows the electron density variation with input RF powers using the 20 mm discharge tube on the center (r=0 mm) of the exit plane (z=0 mm). The relative electron densities are derived from the intensities of 811.5311 nm line and 750.3869 nm line and the absolute electron densities are derived from the RF compensated Langmuir probe with different input RF powers ranged from 50-1600 W. It shows a well good agreement of the relative electron densities derived from OES emission lines and the absolute electron densities derived from the Langmuir probe.

Figure 5 shows the linear relationship of the electron density derived from the Langmuir probe and the 811.5311 nm line intensity derived from the OES, which plots a linear relation that is $n_e=kI_{ij}$ where the unit of n_e is m^{-3}, the coefficient k and emission intensity I_{ij} are just numerical values without units. From a linear fit of the electron density, we can determine the value of k, which is 1.18×10^{13} with a standard error of 4%. Assuming that the electron temperature is constant, the rate coefficient k_{Ar}^{dir} will be the same. Also assuming a constant neutral density distribution, the coefficients in equation (6) will be fix values. Therefore, the k value in equation (7) will be constant and it is applicable for different input RF powers in different diameter discharge tubes as long as the electron temperature is constant. This constant electron temperature assumption is also justified by the experiment results as described following.

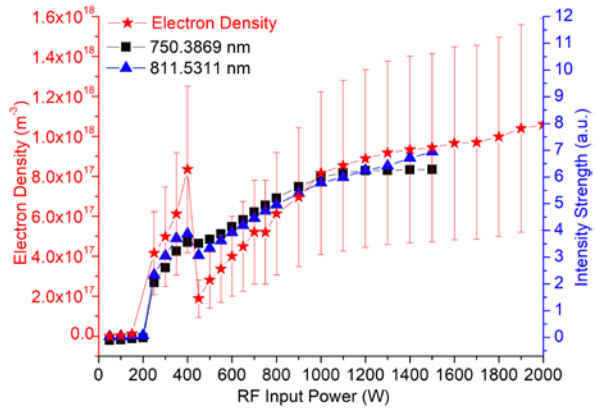

Figure 4. Agreement of the intensity of OES emission lines with electron density derived from the single Langmuir probe.

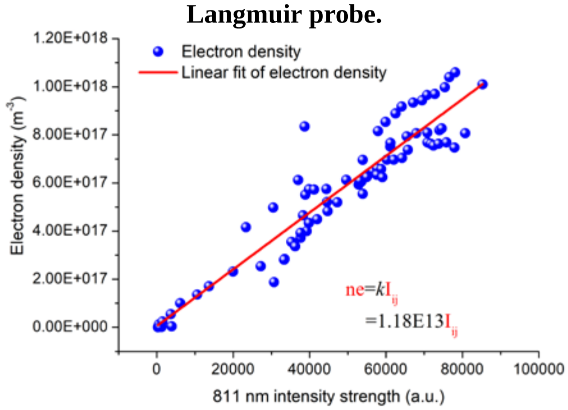

Figure 5. Calibration of the electron density from the Langmuir probe and OES.

B. Spatial Beam Plasma Expansion with Different RF Powers

Figures 6 and 7 show respectively the radial profiles and contour map of the electron density derived from the OES method. The axial distances (z-axis) are indicated by 0-10 cm both in profiles and contour maps. These tests were performed at the discharge tube of 20 mm with a RF input power of 100 W. We can see from these pictures that the maximum electron density locates on the centerline near the exit plane of the discharge tube. The electron density is symmetric with the centerline of the discharge tube and decreases with the increase of both radial and axial distances.

Figures 8 and 9 show respectively the radial profiles and contour map of the electron temperature calculated from the intensity ratio of the 811.5311 nm line and 750.3869 nm line. The electron temperature is about 3.5 eV, it remains nearly constant with the increasing radial and axial distances indicating a isothermal beam plasma expansion.

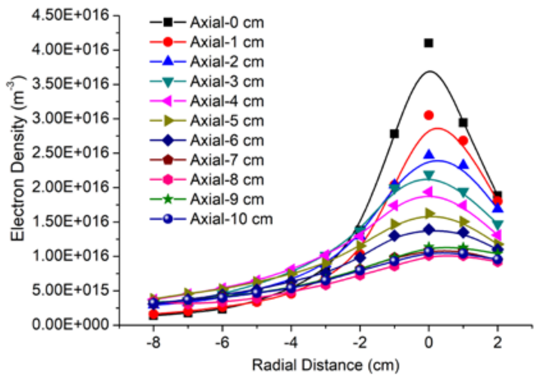

Figure 6. Radial and axial electron density profiles with 20 mm diameter discharge tube and 100 W RF input power.

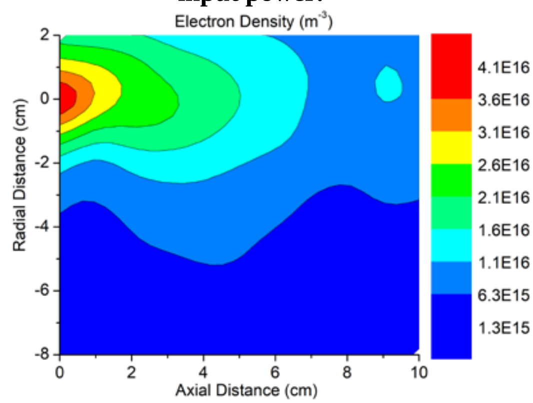

Figure 7. Contour map of electron density with 20 mm diameter discharge tube and 100 W RF input power.

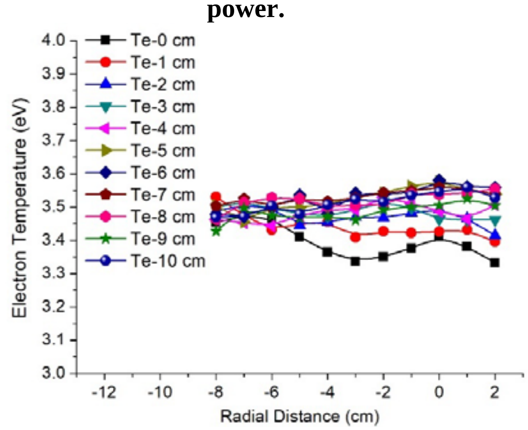

Figure 8. Radial and axial electron temperature profiles with 20 mm diameter discharge tube and 100 W RF input power.

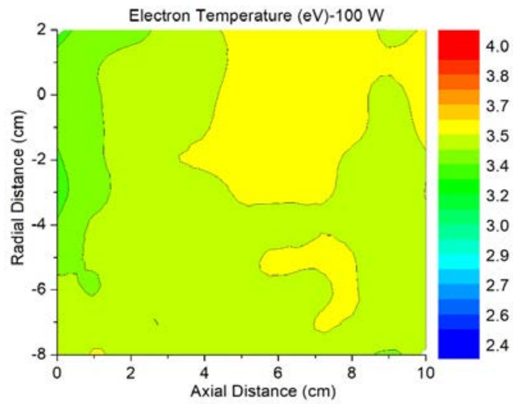

Figure 9. Contour map of electron temperature with 20 mm diameter discharge tube and 100 W RF input power.

Figures 10 and 11 respectively show the radial profiles of the electron density and electron temperature with different RF input powers (100, 600 and 1000 W). We can see from figures 10 and 11 that the centerline electron density increases a lot but the electron temperature remains nearly constant with increasing RF input powers.

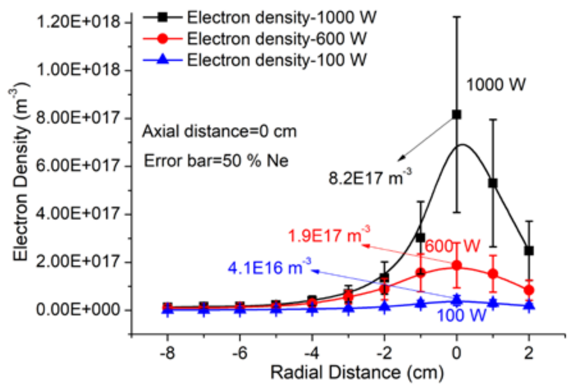

Figure 10. Radial electron density profiles with different RF input powers

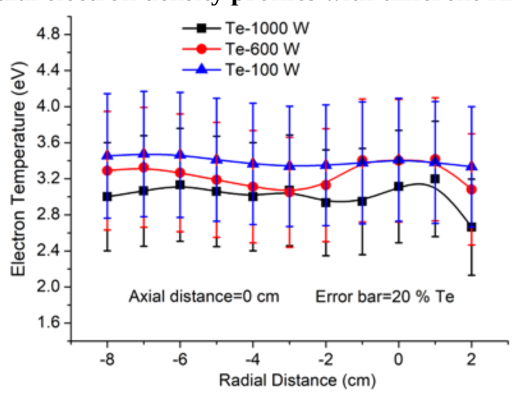

Figure 11. Radial electron temperature profiles with different RF input powers.

C. Spatial Beam Plasma Expansion with Different Diameters of the discharge tube

Figures 12 and 13 show respectively the contour maps of electron density with 40 and 60 mm diameter discharge tubes with the RF input power of 100 W. Compared with the density contour map of the 20 mm diameter discharge tube under the same RF power, as shown in figure 7, the electron density expands along the radial distance as the diameter of the discharge tube getting larger. The axial gradient of the electron density remains almost the same.

Figures 14 and 15 show respectively the contour maps of electron temperature with 40 and 60 mm diameter discharge tubes with the RF input power of 100 W. Compared with the electron temperature contour map of the 20 mm diameter discharge tube under the same RF power, as shown in figure 9, the variation of the electron temperature in both radial and axial directions is very small, in the range of 3.4-3.8 eV, within the 20 % error bar.

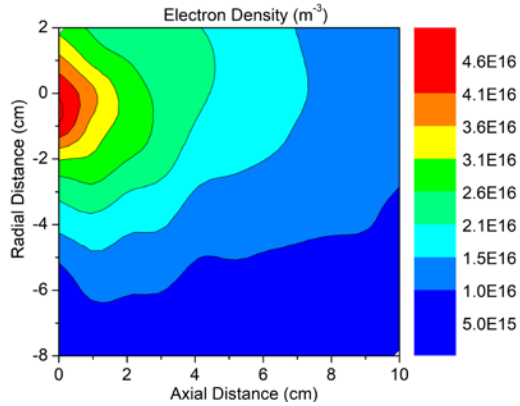

Figure 12. Contour map of electron density with 40 mm diameter discharge tube and 100 W RF input power.

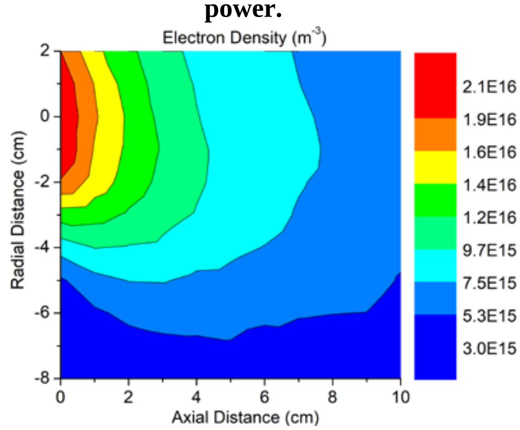

Figure 13. Contour map of electron density with 60 mm diameter discharge tube and 100 W RF input power.

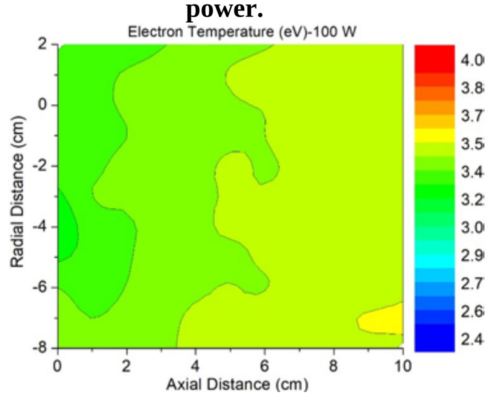

Figure 14. Contour map of electron temperature with 40 mm diameter discharge tube and 100 W RF input power.

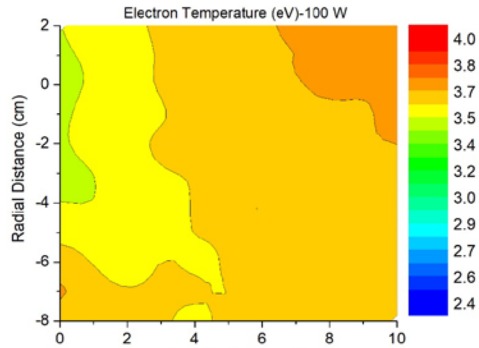

Figure 15. Contour map of electron temperature with 60 mm diameter discharge tube and 100 W RF input power.

Figures 16 and 17 respectively show the radial profiles of the electron density and electron temperature with 20 mm, 40 mm and 60 mm diameters of discharge tube with the RF input power of 100 W. Figure 16 shows that the maximum electron density in the centerline increases and the radial profile concentrates towards the centerline with a smaller diameter of the discharge tube. The radial distribution of the electron density is more uniform with 60 mm diameter of the discharge tube, which is a beneficial property for an electric propulsion thruster. Figure 17 shows that the electron temperature is almost constant for the 20, 40, and 60 mm tubes. These phenomena could be explained as following: the volume of the discharge increases when the diameter of the discharge tube increases, while the RF input power is the same, therefore the input power density decreases leading to a lower density profile. While the electron temperature remains nearly the same.

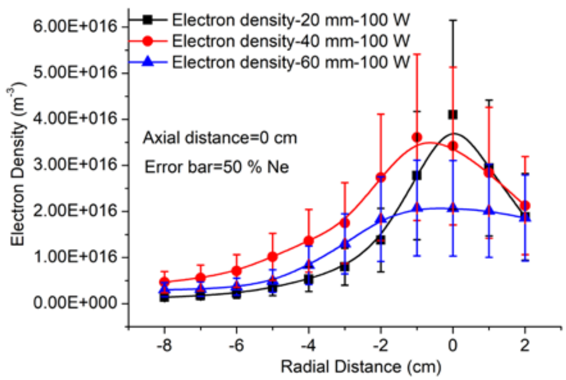

Figure 16. Radial electron density profiles with different diameter of tubes.

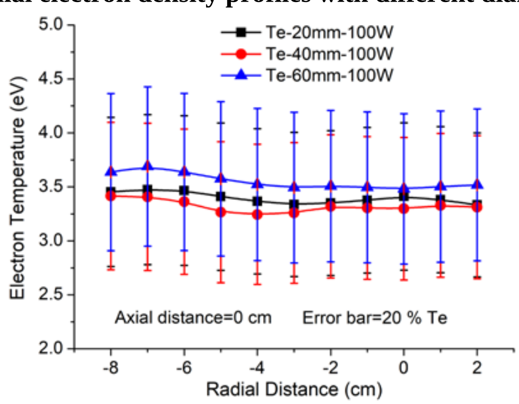

Figure 17. Radial electron temperature profiles with different diameter of tubes.

V. Conclusion

Both the Langmuir probe and the spatially resolved optical emission spectroscopy (OES) have been used for the determination of the electron temperature and density of an argon helicon discharge. Test results show that the intensity of the emission spectra has a good linear relationship with the electron density calculated from the Langmuir probe.

Beam plasma expansion contour maps on different working conditions of the helicon source have been plotted. Test results show that the electron density increase with the increasing RF input powers and decrease with the increasing diameters of the discharge tube. But, the electron temperature remains almost constant with different RF input powers and diameters of the discharge tube. This result indicates that the beam plasma follows a isothermal or a Boltzmann expansion.

Acknowledgments

This work was supported by the National Natural Science Foundation of China (Grant No. 11805011 and 11872093)

References

[1] C Charles, "A review of recent laboratory double layer experiments", Plasma Sources Sci. Technol., 16 (R1–R25), 2007.

[2] C Charles, W Cox, R W Boswell, R Laine and M Perren, "Experimental investigation of a conical helicon double layer thruster arrangement", Plasma Sources Sci. Technol., 19 (045003), 2010.

[3] C. Charles, "High source potential upstream of a current-free electric double layer", Physics of Plasmas, 12 (044508), 2005.

[4] Michael D West, Christine Charles and Rod W Boswell, "High density mode in xenon produced by a Helicon Double Layer Thruster", J. Phys. D: Appl. Phys., 42 (245201), 2009.

[5] Christine Charles and Rod W. Boswell, "Effect of Exhaust Magnetic Field in a Helicon Double-Layer Thruster Operating in Xenon", IEEE Transactions on Plasma Science, 36 (5):2141-214, 2008.

[6] Francis F. Chen, "Permanent Magnet Helicon Source for Ion Propulsion", IEEE Transactions on Plasma Science, 36 (5):2095-2110, 2008.

[7] Benjamin W. Longmier at el., "VASIMR® VX-200 Performance Measurements and Helicon Throttle Tables Using Argon and Krypton", IEPC-2011-156.

[8] Juan Del Valle, at el., "Measurement of the Dielectric Wall Erosion in Helicon Plasma Thrusters: an Application to the VASIMRR VX-CR Experiment", IEPC-2013-188.

[9] W. Cox, C. Charles, R. W. Boswell, and R. Hawkins, "Spatial retarding field energy analyzer measurements downstream of a helicon double layer plasma", Applied Physics Letters, 93(071505), 2008.

[10] Logan Todd Williams, "Ion Acceleration Mechanisms of Helicon Thrusters", PhD. thesis, Aerospace Engineering, Georgia Institute of Technology, Atlanta, GA, 2013.

[11] Kazunori Takahashi, Daiki Sato, Koichi Takaki and Akira Ando, "Development of a compact magnetically expanding plasma source with a strong magnetic field", Plasma Sources Sci. Technol., 22(055002), 2013.

[12] K. Behringer, "Diagnostics and modelling of ECRH microwave discharges", Plasma Physics and Controlled Fusion, 33(9):997-1028, 1991.

[13] G. Crolly and H. Oechsner, "Comparative determination of the electron temperature in Ar- and N2-plasmas with electrostatic probes, optical emission spectroscopy OES and energy dispersive mass spectrometry EDMS", Eur. Phys. J. AP 15:49-56, 2001.

[14] M. V. Malyshev and V. M. Donnelly, "Determination of electron temperatures in plasmas by multiple rare gas optical emission, and implications for advanced actinometry", Journal of Vacuum Science & Technology A, 15(3):550-558, 1997.

[15] Hans R. Griem, "Validity of Local Thermal Equilibrium in Plasma Spectroscopy", Physical Review, 131(3):1170-1176, 1963.

[16] T Czerwiec and D B Graves, "Mode transitions in low pressure rare gas cylindrical ICP discharge studied by optical emission spectroscopy", J. Phys. D: Appl. Phys. 37:2827–2840, 2004.

[17] Gao Zhao, Huihui Wang, Xinlu Si, Jiting Ouyang, Qiang Chen, and Chang Tan, "The discharge characteristics in nitrogen helicon plasma", Physics of Plasmas 24, (123507), 2017.

[18] Gao Zhao, Wanying Zhu, Huihui Wang, Qiang Chen, Chang Tan and Jiting Ouyang, "Study of axial double layer in helicon plasma by optical emission spectroscopy and simple probe", Plasma Sci. Technol. 20 (075402), 2018.

[19] Francis F. Chen, "Lecture Notes on Langmuir Probe Diagnostics", Mini-Course on Plasma Diagnostics, IEEE-ICOPS meeting, Jeju, Korea, June 5, 2003.

[20] Robert B. Lobbia and Brian E. Beal, "Recommended Practice for Use of Langmuir Probes in Electric Propulsion Testing", J Propul Power, 33(3):566-581, 2017.

[21] Herman D A and Gallimore A D, "A High-Speed Probe Positioning System for Interrogating the Discharge Plasma of a 30 cm Ion Thruster", AIAA Paper, 2002-4256, 2002.

[22] Herman D A, McFarlane D S and Gallimore A D, "Discharge Plasma Parameters of a 30-cm Ion Thruster Measured without Beam Extraction using a High-Speed Probe Positioning System", IEPC 2003-0069, 2003.

[23] Zun Zhang at el., "Steady and oscillatory plasma properties in the near-field plume of a hollow cathode", Plasma Sci. Technol. 20 (024010) , 2018.

[24] A. W. Degeling, C. O. Jung, R. W. Boswell, and A. R. Ellingboe, “Plasma production from helicon waves”, Physics of Plasmas, 3(2788), 1996.